Tech Science Press

Design and Manufacture of Bionic Porous Titanium Alloy Spinal Implant Based on Selective Laser Melting (SLM)

Xiaojun Chen[1], Di Wang[1,*], Wenhao Dou[1], Yimeng Wang[1], Yongqiang Yang[1], Jianhua Wang[2] and Jie Chen[1]

[1]School of Mechanical and Automotive Engineering, South China University of Technology, Guangzhou, 510641, China
[2]Hospital of Orthopedics, Guangzhou General Hospital of Guangzhou Military Command, Guangzhou, 510010, China
*Corresponding Author: Di Wang. Email: mewdlaser@scut.edu.cn

Abstract: In order to meet the clinical requirements of spine surgery, this paper proposed the exploratory research of computer-aided design and selective laser melting (SLM) fabrication of a bionic porous titanium spine implant. The structural design of the spinal implant is based on CT scanning data to ensure correct matching, and the mechanical properties of the implant are verified by simulation analysis and laser selective melting experiment. The surface roughness of the spinal implant manufactured by SLM without post-processing is Ra 15 μm, and the implant is precisely jointed with the photosensitive resin model of the upper and lower spine. The surface micro-hardness of the implant is HV 373, tensile strength σ_b = 1238.7 MPa, yield strength $\sigma_{0.2}$ = 1043.9 MPa, the elongation is 6.43%, and the compressive strength of porous structure under 84.60% porosity is 184.09 MPa, which can meet the requirements of the reconstruction of stable spines. Compared with the traditional implant and intervertebral fusion cage, the bionic porous spinal implant has the advantages of accurate fit, porous bionic structure and recovery of patients, and the ion release experiment proved that implants manufactured by SLM are more suitable for clinical application after certain treatments. The elastic modulus of the sample is improved after heat treatment, mainly because the microstructure of the sample changes from α' phase to α + β dual-phase after heat treatment. In addition, the design of high-quality bionic porous spinal implants still needs to be optimized for the actual needs of doctors.

Keywords: Selective laser melting (SLM); titanium; spinal implant; bionic porous

1 Introduction

With the development of surgical techniques, many complex surgical procedures have been successfully implemented. Spinal surgery is a cutting-edge of orthopedic surgery, the spine is around with important nerves and blood vessels and the spinal canal also contains the spinal cord. Therefore, only to achieve accuracy in the operation process can ensure the safety of surgery. During the procession of spinal surgery in spinal tumor, spinal deformity and intervertebral disc disease, the lesions often need to be

thoroughly removed, and displaced by a support structure (implant) in order to maintain the stability and integrity of the spine [1–2].

In terms of metal 3D printing technology for human implants, clinical applications are still less, one of the main reason is that the current metal 3D printing technology is not mature, printing materials, printing precision is not enough to support the clinical application; another reason is that medical 3D printing technology involves physics [3–4], material science [5–6], medical [7] and computer and other disciplines. There are huge needs for cooperation with biological engineering, biological materials, image processing, computer modeling, and other clinical specialist professionals in the field, but there is still a lack of research centers and institutions related to the cooperation of human resources together, which restrict the translation of metal 3D printing implant from research to clinical. Since 1983, Bagby and Kuslish have developed a BAK fusion cage for lumbar intervertebral fusion in humans [8–9], various spinal implants for spinal reconstruction has developed. At present, allograft bone spine implants are mainly titanium mesh cage [10–11] polyetheretherketone (PEEK) fusion cage [12–13], composite bone [14], etc. The current commonly used medical implants have the following problems: firstly, the implant is a standard part, which does not fully meet the patient's anatomy, or needs to be cut, pre-bended during the operation, causing a reduction of the operation effect [15]; secondly, the elastic modulus of solid metal spinal implant is large, which is easy to cause stress shielding and adjacent segment degeneration [16]; thirdly, spinal implant is not easy to fix between the upper and lower spine, which may lead to surgical failure [15].

There are many traditional manufacturing methods for making porous implants, including powder sintering [17], freeze casting [18] and polymer sponge replacement [19]. However, these methods cannot guarantee the dimensional accuracy and void structure of the implant, nor can they guarantee the connectivity of the internal holes. The laser selective melting technology (Selective Laser Melting, SLM) uses the computer-aided method to design and manufacture. The complex 3D model was designed, sliced and then manufactured with the principle of laminated manufacturing [20]. SLM technology can nearly manufacture parts with arbitrary shape owing to it's shaping principle. With the continuous development of SLM technology, the manufacturing precision and effects are getting better. SLM technology has the advantages of direct forming of a complex surface, a porous structure, which means a huge potential in the field of surgery [21–22].

The case discussed in this paper is designing a bionic porous titanium spine implant to meet the needs of spinal surgery, and verifying the feasibility of this scheme by computer-aided design and SLM rapid prototyping. The key of this article is to study the design and manufacture of bionic porous spinal implant with SLM, and some exploratory experiments were conducted to design the implant. Beside, the surface roughness, micro-hardness, tensile and compressive strength, toxic ion release were also discussed. Accuracy is verified by the simulation matching experiment, the elastic modulus and other key indicators are not included in the scope of discussion.

2 Personalized Design of Bionic Porous Spinal Implant

A human spinal biological specimen was selected as the research object. The study was performed to remove the epistropheus and to reconstruct the spinal stability with a new intervertebral fusion cage. The CT scanning was performed to obtain the CT scanning data, and the following steps were designed.

2.1 Personalized Design Steps of Spinal Implant

Step one: the extraction and processing of target spine model

Importing CT scanning data of patients to Mimics 15.01 software, then stored as STL format data into Geomagic software to eliminate noise model, and further obtain the operation of three-dimensional entity
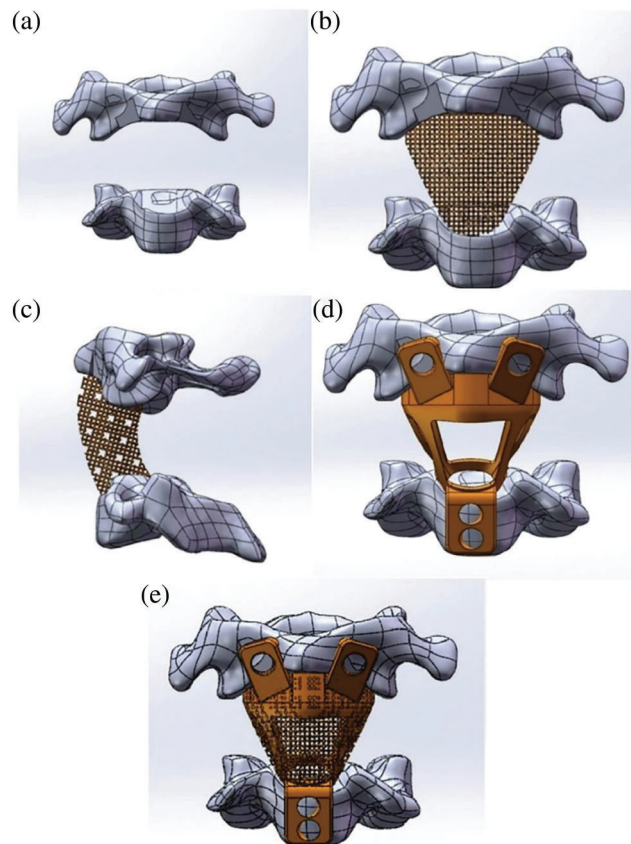
Figure 1: Design of spinal implant, a) target spine model; b) bionic porous structure; c) bionic porous structure (side view); d) shell structure of implant; e) design sketch of the implant

model in STEP format; then the data will be saved and transferred to the SolidWorks 3D design software, and the target model can be obtained, as shown in Fig. 1a.

Step two: Design of bionic porous implant subject

To construct a bionic porous structure between target surfaces. The average pore diameter of the porous structure is 300–1000 µm, which is more conducive to the ingrowth of human bone tissue [23]. Considering the size limitation of SLM manufacturing, the bionic porous structure is designed with two pore structures, which are 0.75 mm and 1.5 mm respectively, as shown in Figs. 1b and 1c. The porous structure designed in this paper uses two levels of porous form, that is, in an orderly arrangement of porous structure, and then add porous structure with different pore diameter, form a two kinds of pore structure including stage one and stage two, which are more conducive to human tissue ingrowth into the implant, conducive to patient recovery. The porous structure is hollow inside the body and an internal channel was constructed to facilitate the implantation of some artificial bone or autogenous bone during the operation of the surgeon, and then to guide the recovery and growth of bone tissue. In order to make the connection between the vertebral implant and the adjacent vertebra can be more stable, the joint surface of the implant and the third section spine was designed for the plane, and the third section spine was slightly cut, which is a common practice for surgeons to increase the effectiveness of surgery.

Step three: Design of implant system into shell

To achieve a good reconstruction of the spine to be stable with a spinal implant can not only rely on bionic porous structure, therefore, it is necessary to construct fixed screw holes connected between the shell supporting the porous structure and the upper and lower spine, as shown in Fig. 1d.

Step four: The overall design of implant

The porous structure is combined with the supporting part of the shell to form the final implant and fillet operations were also carried out, as shown in Fig. 1e.
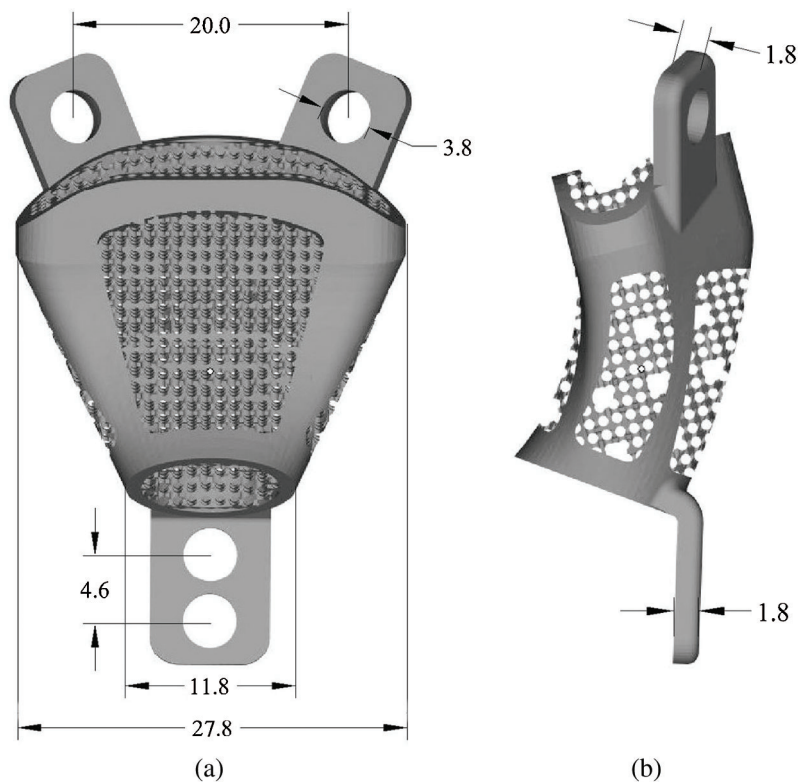
2.2 Geometric Parameters Design of Spinal Implant

The geometric parameters of the implant are shown in Tab. 1:

As shown in Fig. 2, the shell which supports the porous structure is designed with a thickness of 1.8 mm, and the inner bionic porous structure is obtained by removing the circular hole in three orthogonal directions. The diameter of the first stage pore is 0.75 mm, and the diameter of the second stage pore is 1.5 mm. The vertical height is 44.55 mm.

Table 1: Geometric parameters of spinal implant

|	Maximum cross-section size/mm	The distance between fixed holes/mm	The thickness of fixed plate/mm	Diameter of fixed holes/mm
Atlas binding face	27.8	20.0	1.8	3.8
Third intervertebral binding face	11.8	4.6	1.8	3.8

Figure 2: Geometric parameters of spinal implant(mm): (a) Front side; (b) Right side

3 Experimental Methods

3.1 Finite Element Analysis

1. Establishment of finite element model

In this study, the mechanical properties of the porous structure model are analyzed with the help of the finite element analysis software Workbench19.0. The finite element analysis adopts the model with the same pore structure as the implant, but the porosity of the four models is different. The porous structure is modeled in a space with a diameter of 10 mm and a height of 10 mm, as shown in Fig. 3. The primary holes along the X, Y, and Z axes are equidistant with spacing d. The secondary hole only exists in the XOY plane and the XOZ plane, and the center of the hole is located at the midpoint of the straight line between the centers of the two primary holes, as shown in Fig. 3b, the red circle is the primary hole and the blue circle is the secondary hole. The spacing of secondary holes is 3d in the XOY plane and 4d in the XOZ plane. By adjusting the layout spacing d, the total porosity of the structure is obtained, and the design parameters of different porosity are shown in Tab. 2.
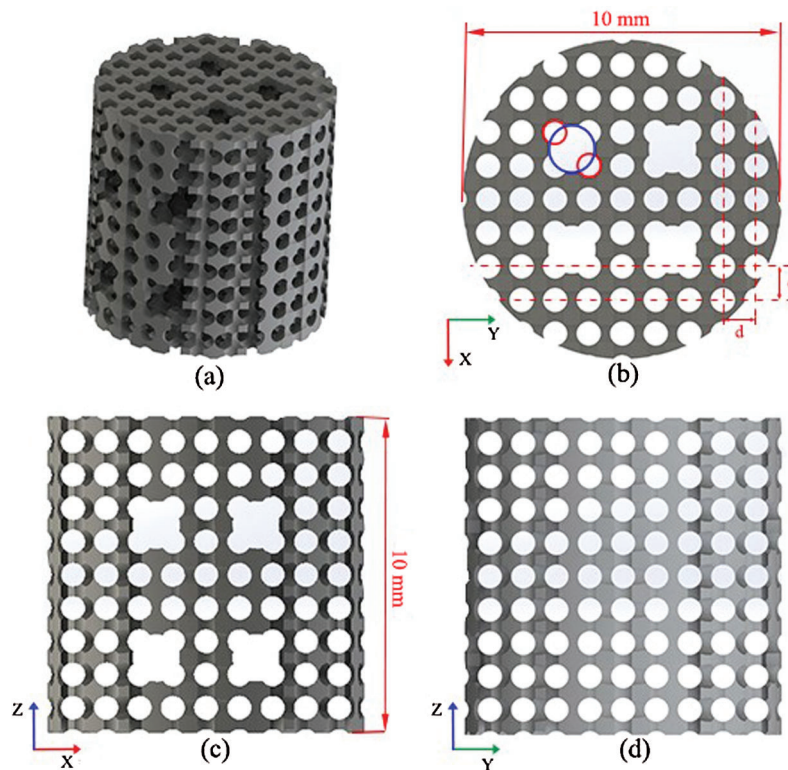
Figure 3: Porous structure design: (a) Isometric view, (b) Top side, (c) Right side, (d) Front side

Table 2: Design parameters of different porosity structure

Porosity	Primary hole size/mm	Secondary hole size/mm	Array spacing d/mm
69.3%	0.75	1.5	1.10
75.3%			1.00
80.4%			0.95
84.6%			0.87

In the establishment of the model, the following assumptions are made: (1) there are no cracks, holes and other defects in the SLM forming process, and the material used is an ideal material with stable performance; (2) the implant is subjected to uniform force in the human body.

2. Material properties and meshing

The material properties of the finite element model are set to the material properties of Ti6Al4V, which as shown in Tab. 3. In the process of analysis, it is assumed that the material is isotropic and the hardening characteristics of the material are taken into account, so it is defined as a Multilinear Kinematic hardening material model [24]. In this study, we hope to obtain the stress distribution and deformation of the model through simulation analysis, so as to know which positions in the model are prone to failure. Therefore, we only carry out elastic analysis. The equilibrium equations of elasticity can be expressed as:

Table 3: Material parameters used in simulation

Parameters	Elastic modulus (Gpa)	Poisson's ratio	Yield strength (Mpa)	Ultimate strength (Mpa)
Value	110	0.34	960	1200

$$\frac{\partial \sigma_x}{\partial x} + \frac{\partial \tau_{xy}}{\partial y} + \frac{\partial \tau_{xz}}{\partial z} + f_x = 0$$

$$\frac{\partial \tau_{yx}}{\partial x} + \frac{\partial \sigma_y}{\partial y} + \frac{\partial \tau_{yz}}{\partial z} + f_y = 0 \tag{1}$$

$$\frac{\partial \tau_{zx}}{\partial x} + \frac{\partial \tau_{zy}}{\partial y} + \frac{\partial \sigma_z}{\partial y} + f_z = 0$$

where σ and τ are nominal stress and shear stress, respectively. f_x, f_y and f_z are body force com-ponents in the three directions of x, y and z, respectively. In the state of three-dimensional stress, the constitutive equation of elastic strain can be expressed as:

$$\begin{Bmatrix} \sigma_x \\ \sigma_y \\ \sigma_z \\ \tau_x \\ \tau_y \\ \tau_z \end{Bmatrix} = G \begin{Bmatrix} 1-v & v & v & 0 & 0 & 0 \\ v & 1-v & v & 0 & 0 & 0 \\ v & v & 1-v & 0 & 0 & 0 \\ 0 & 0 & 0 & \frac{1-2v}{2} & 0 & 0 \\ 0 & 0 & 0 & 0 & \frac{1-2v}{2} & 0 \\ 0 & 0 & 0 & 0 & 0 & \frac{1-2v}{2} \end{Bmatrix} \begin{Bmatrix} \varepsilon_x \\ \varepsilon_y \\ \varepsilon_z \\ \gamma_{xy} \\ \gamma_{yz} \\ \gamma_{zx} \end{Bmatrix} \tag{2}$$

in which

$$G = \frac{E}{(1+v)(1-2v)} \tag{3}$$

where E is the elastic modulus, v is the poisson's ratio, ε and γ are nominal strain and shear strain

In order to improve the simulation efficiency while ensuring the accuracy of the simulation results, the finite element model is meshed by quadratic tetrahedron [24], and the total number of mesh nodes and elements as shown in Tab. 4.

Table 4: The number of nodes and elements with different porosity

| Porosity	69.3%	75.3%	80.4%	84.6%
Number of nodes	563514	559930	472095	942720
Number of elements	320516	312160	250996	508787

3. Boundary condition

The boundary conditions in the process of analysis are shown in Fig. 4, in which a fixed support is added to the bottom surface of the model while those of the upper surface were bonded to a rigid plate where a compression force producing a vertical distributed load. This study focuses on the stress simulation analysis of porous structures, so the analysis is limited to the range of linear elastic deformation.
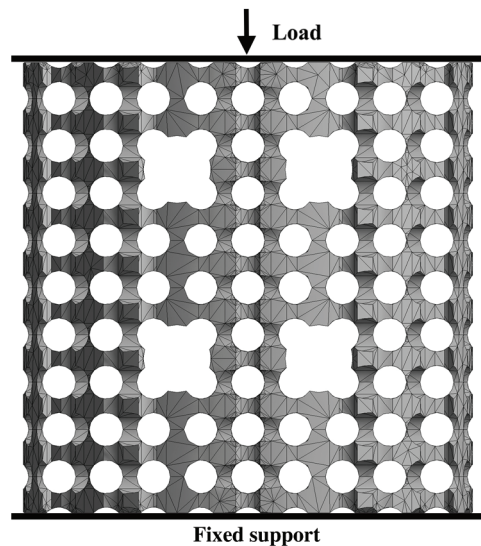
Figure 4: The generated meshes and the boundary conditions for models

During running, the pressure on the spine is six times greater than usual. If the daily pressure is 500 N, the pressure of 3000 N will be generated during running. Therefore, this paper sets the load to 3000 N for simulation analysis, and the maximum loading force is equally divided into 50 sub-steps to load on the analytical model within 1 s. Other simulation settings use the default options of the software.

3.2 Equipment, Materials and Process Parameters

The manufacturing process is completed by the SLM equipment DiMetal-100, which is developed by South China University of Technology, as shown in Fig. 5. The core parts of the equipment are mainly fiber laser, an optical system, sealing chamber, powder system, control system and process software. By scanning the galvanometer, the laser can be used for selective scanning of the powder in the working chamber, so as to manufacture metal parts layer by layer. The main technical parameters of the equipment are as follows: 200 W laser power (maximum), spot diameter about 70 μm, scanning speed range of 10–5000 mm/s, layer thickness range of 20–100 μm, the maximum manufacturing size of 100 mm × 100 mm × 120 mm. In the manufacturing process, metal powder has undergone the process of melting and re-solidification. In order to prevent the manufactured parts from oxidizing in this process, it is necessary to pass an inert gas such as nitrogen or argon in the working chamber to ensure that the oxygen content in
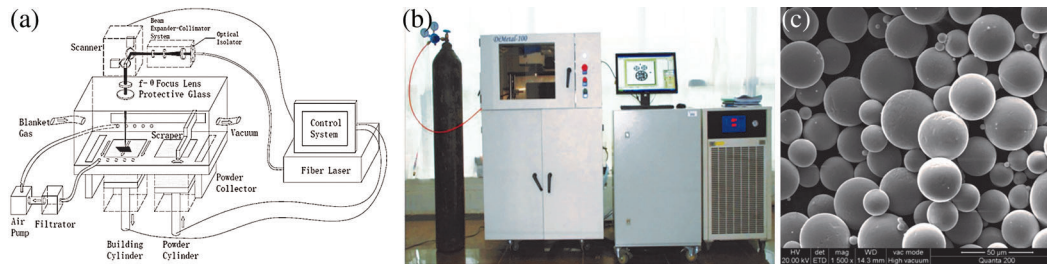
Figure 5: SLM manufacturing principle and a) SLM principle; b) SLM equipment, c) Micro-topography of Ti6Al4V powder

the chamber is 0.15% to ensure that the manufacturing efficiency. In this paper, we use the medical grade Ti6Al4V powder produced by Wuxi Firecomms company, China. The powder is spherical, as shown in Fig. 7c. The average particle size is 35.18 μm, Composition of Ti6Al4V powder: Ti (89.27%), Al (5.85%), V(3.99%), and the powder oxygen content is about 600 ppm.

Based on the parameter optimization [25], the manufacturing parameters of Ti6Al4V powder are set as follows: laser power is 150 W, scanning speed is 400 mm/s, scanning distance is 0.08 mm, layer thickness is 30 μm, S-shaped cross scanning mode, high purity argon shielding gas.

3.3 Experiment Procedure

1. A three-dimensional model of a biomimetic porous spinal implant was designed with the assistance of a surgeon according to the aforementioned method;

2. The model is exported to Magics15.01 software in STL format and trimmed. Because of the porous structure inside the implant, it is very difficult to add support directly. So here we choose the smaller combination of implant to face down, and the internal porous structure is added between the bonding surface and the substrate in the form of support, so as to ensure the quality of most parts of the implant, as shown in Fig. 7a. At the same time, the traditional machining method is adopted directly to the lower joint surface when the support is removed. Because the lower joint surface is designed to be a plane, the machine can ensure the effect of the implant;

3. The spot compensation and layer thickness are set up for the model and support by Magics15.01 software, and the slice data and path planning data will be exported after slicing;

4. The data is imported into the SLM equipment, the quality of the process was evaluated after manufacturing, and the surface of the implant will be sandblasted and polished to check the matching degree of the implant.

3.4 Testing Methods

The surface roughness Ra of the implant was measured by using a desktop ultra-precision three-nnnand a vertical measurement repeat rate of <0.02 nm. The sampling length is 0.8 mm, the testing length is 4 mm, and the sampling speed is 0.05 mm/s. The micro-hardness was measured with a digital micro-hardness tester HVS-1000 with a resolution of 0.01 μm and a measurement range of 1 HV-3000 HV. The tensile properties and compression properties were measured by using the CMT5105 Electronic Universal Tester.

Because Al and V are the most primary toxic elements in medical titanium alloys, a long-term implantation in organism will release Al and V ions. Therefore, the ion release experiment needs to be carried out, and the ion release of Al and V ions in the SLM-manufactured titanium alloy implant was measured by UV500 UV-vis spectrophotometer to evaluate the biocompatibility of SLM titanium alloy implant [26] and to determine whether it can replace traditional standard implant for human implantation.

4 Results and Discussions

4.1 Finite Element Analysis Results

The elastic moduli of different porosity models are obtained from the simulation results. As shown in Tab. 5, the elastic modulus decreases with the increase of porosity, and the maximum elastic modulus is only 12.6 Gpa, which greatly reduces the elastic modulus of the material. The von-Mises stress cloud diagram of different porosity models under 3000 N load is shown in Fig. 6. It can be seen from the diagram that the maximum von-Mises stress appears on the pore strut parallel to the load direction under different porosity. At the same time, the maximum von-Mises stress decreases at first and then increases with the increase of porosity, and the minimum value is obtained when the porosity is 80.4%. It can be clearly seen from Fig. 6 that the stress distribution of the structure is more uniform when the porosity is 80.4%, while the stress concentration is more likely to lead to failure when the porosity is 69.3% and 84.6%. One of the reasons for the stress concentration is that there is an unsmooth excess in the porous structure, which leads to the sudden change of stress, and the other reason is that the rod diameter is too small, which leads to more pressure in a certain direction and then produce more stress.

Table 5: Elastic modulus of different porosity models

Porosity	69.3%	75.3%	80.4%	84.6%
Elastic modulus (Gpa)	12.6	9.2	7.5	5.6
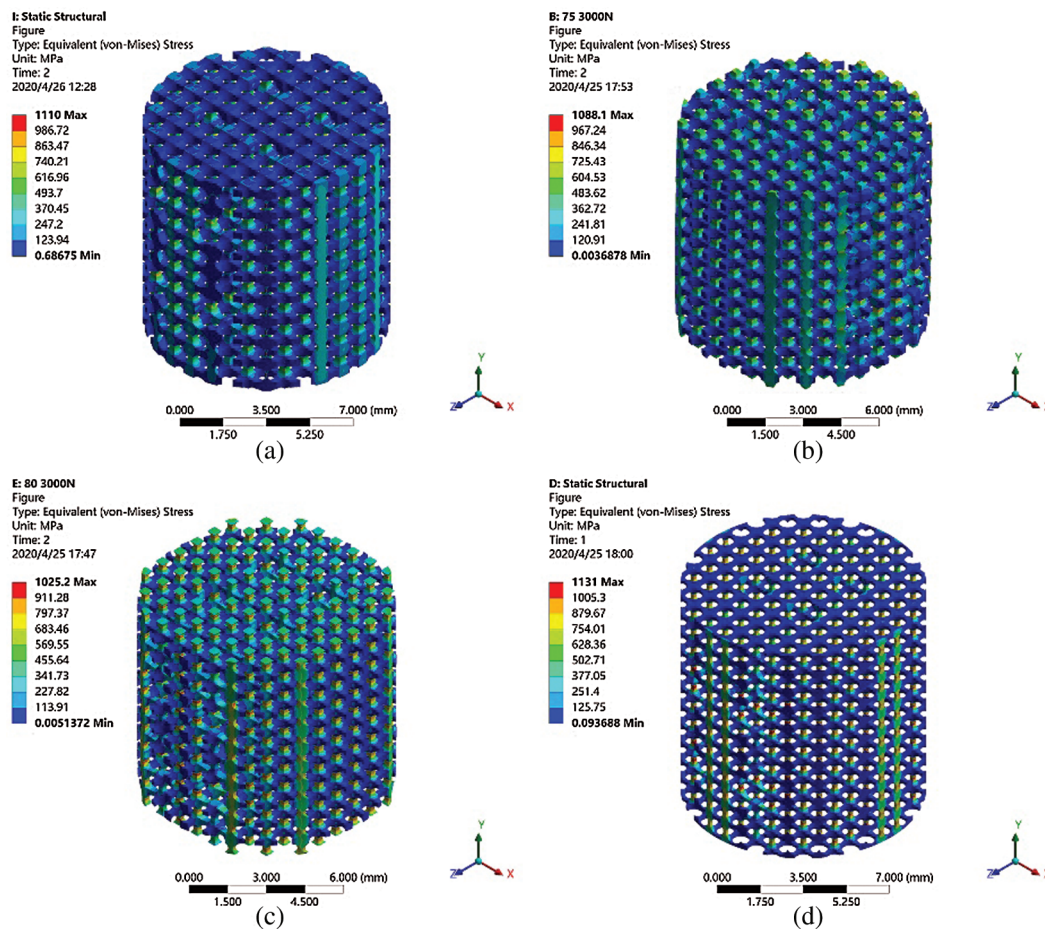
Figure 6: Equivalent stress of different porosity models: (a) 69.3%, (b) 75.3%, (c) 80.4%, (d) 84.6%

Under the same load, the deformation of each model is shown in Fig. 7. It can be seen from the figure that the deformation of the model increases with the increase of porosity. The model with small porosity has a large elastic modulus and a strong ability to resist deformation, so the total deformation is small. The structures with four kinds of porosity all show that there is a larger deformation in the upper part of the structure, so it can be inferred that in the actual compression process, the upper part of the model is more likely to fail, and the collapse propagates layer by layer to achieve compaction.
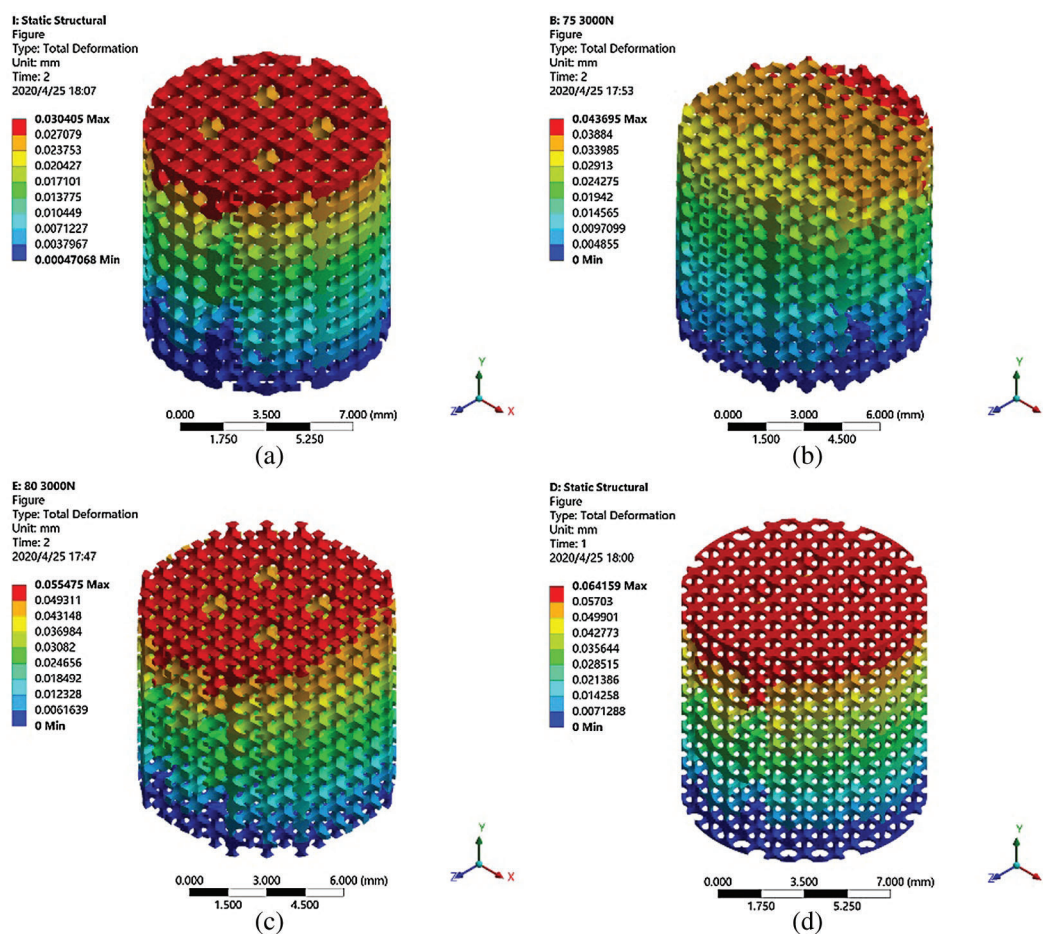

Figure 7: Total deformation of different porosity models: (a) 69.3%, (b) 75.3%, (c) 80.4%, (d) 84.6%

4.2 The Effect of Porous Spinal Implants Manufactured by SLM

The manufacturing effect of the implants are shown in Fig. 8b.

From the perspective of the entity, the SLM manufacturing effect is good, with no obvious defects. Fig. 8c shows the microstructure of the internal porous structure, it's visible that the circular shape is consistent with the actual design, the actual size of the first stage hole is 0.70 ± 0.07 mm, and the actual size of the second stage hole is 1.41 ± 0.07 mm. There is a slight deviation between the actual aperture size and the design aperture, in which the actual aperture size is actually smaller. A small amount of powder adhesion exists in the holes, which affects the hole size to some extent. This is because the laser spot diameter is about 70 μm, a certain width of melting channel will be formed in the manufacturing process, the powder on the edge of melting path is prone to adhesion which is a principle error of SLM manufacturing.
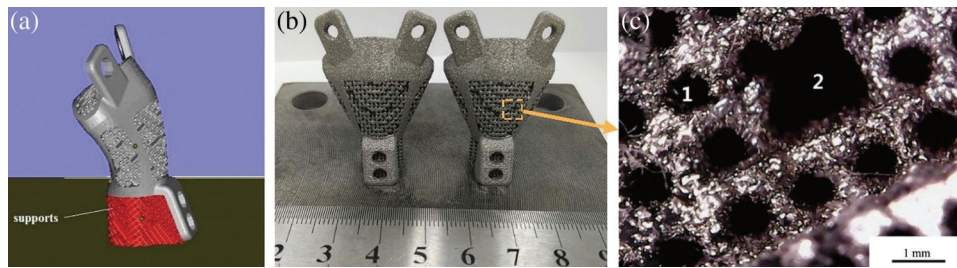
Figure 8: Support adding and SLM manufacturing of implant: a) support adding result, b) SLM manufacturing result, c) Microscopic characteristics of porous structure (No. 1 is First stage hole, No. 2 is Second stage hole)

4.3 Manufacturing Accuracy and Mechanical Properties

4.3.1 Simulation Matching Experiment

Due to the current domestic related policies and regulations are to be improved, spinal implants manufactured by 3D printing technology are not eligible for market access yet. Therefore, the model of vertebral implant was simulated by resin model to verify the matching degree of the spinal implant. The models of atlas and third vertebrae were printed by 3D Systems company's ProJet6000HD equipment. The printing accuracy of the device was less than 100 μm, and the material used was photosensitive resin. Fig. 9 shows the coordination between the SLM manufactured Ti6Al4V spinal implant and the spinal model of the photosensitive resin. It can be seen that the spinal implant is perfectly coordinated with the resin model, there is no gap between the implant and atlas junction, the implant and the third vertebrae, and the upper and lower joint surfaces are completely constrained on the model. Because the main surface of the implant is the joint surface between the upper and lower vertebrae, the deformation of the rest of the implant is not measured. The measurement results show that the surface roughness of SLM implant is Ra 15 μm which is much higher than that of the traditional processing methods of machining parts. But it still needs further sandblasting and polishing processing which increases the economic and time cost of SLM manufactured parts, and limits the application of SLM technology in some other industrial fields. Through the matching experiment with the resin model, it is verified that the SLM porous implant has good dimensional accuracy.
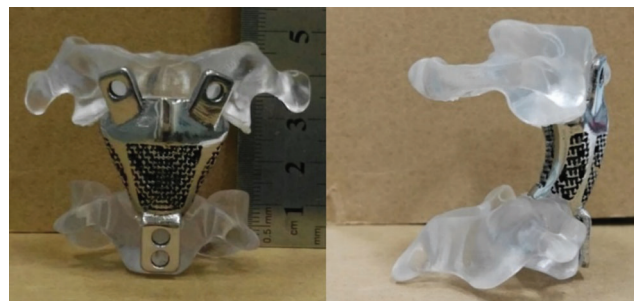
Figure 9: SLM manufacturing intervertebral fusion cage and resin model match

From the surface quality of the implanted implant, some of the surfaces are rough due to the existence of hanging surface. Therefore, designers are required to avoid placing high-surface-quality surfaces in a drape position during data processing. The reason for this phenomenon is that the thermal conductivity of the powder is only 1/100 of the material [20]. In the SLM manufacturing process, the energy of the pure powder support region is much larger than that of the solid in the same process parameters support area,

so that the melting pool of powder support area has become particularly large, due to the role of gravity and capillary force, the surface quality of the overhanging surface is relatively poor.

Since the intervertebral fusion cage is a medical device implanted in human body, it still takes time to apply for an appropriate medical license. As a result, the implantation of the SLM manufactured communicating porous intervertebral fusion cage was demonstrated by biological specimens. The spinal stability was reconstructed by the SLM manufactured intervertebral fusion cage and related skull fixation instruments. In terms of practical use, the intervertebral fusion device eliminates the tedious steps in the construction of prosthesis in the process of implantation, besides, the intervertebral fusion device is planned and manufactured before the operation, and the matching is in good condition. Thus, the SLM manufactured intervertebral fusion cage can provide effective help for clinical application.

4.3.2 Mechanical Properties

Normally, the hardness and compressive strength of the SLM manufactured parts are comparable or even higher than the casting level. But its fatigue performance, surface roughness and elongation and other mechanical properties are poor [4,27–29]. The micro-hardness of SLM manufactured Ti6Al4V implant is HV 373, and the micro-hardness is higher than that of casting which is in line with the expectation.

According to the standard ISO 6892-1:2016, the drawing piece (gauge distance 40 mm, diameter 5 mm) is made of DiMetal-100 equipment with the same process parameters of the implant, and the parts are shown in Fig. 10a. All samples were polished and some samples were treated by heat treatment. Tensile test of the heat-treated tensile part and the non-heat-treated drawing part is carried out, and the data as shown in Tab. 6 are obtained. From the table, the tensile strength of SLM forming titanium alloy specimen without heat treatment is 1238.7 MPa, yield strength is 1043.9 MPa, elongation is 6.43%. Compared with the traditional titanium alloy ASTM F136, the tensile strength and yield strength meet the requirements, but the elongation cannot meet the requirements. It can be observed in Fig. 10c that the heat treatment mainly consists of acicular martensitic α' phase and β phase. After the heat treatment, the α' phase grows in large numbers and is dispersed in the β phase after recrystallization and annealing, as shown in Fig. 10d. This is because when the heat treatment temperature approaches the β phase transition temperature, the β phase nucleates along the α phase boundary. The closer the temperature is to the phase transition temperature, the higher the β phase content. As the acicular martensite α phase transforms into a layered α + β dual-phase structure, the elongation of the material increases accordingly. Eventually, the tensile strength and yield strength of the SLM manufactured titanium alloy parts decreased to some extent, and the elongation increased to 10.18%. All the data met the requirements of medical titanium alloy.

Four compression parts with different porosities are designed, and the DiMetal-100 equipment is used to manufacture the compressed sample of the porous structure according to ISO 13314-2011 standard. Because the second stage pore structure is not the ISO 13314-2011 standard, the compressed sample is manufactured with the first stage pore structure temporarily, and the samples with four kinds of porosity are formed as shown in Fig. 11. Wen CE pointed out that the compressive strength of the porous part of artificial implant should reach 40 MPa [31], it can be seen from Tab. 7 that the minimum compressive strength of the compressed sample under the four kind porosity σ_{bc} = 184.09 MPa, which has met the requirement of the corresponding compressive strength. At the same time, it can be seen from Tab. 7 that the elastic modulus of porous structure with different porosity ranges from 4.92 Gpa to 5.51 Gpa, which matches the elastic modulus of bone.

Compared with the simulation results, the elastic modulus obtained by experiments is twice as small as the simulation results. The main reason is that there are different degrees of micro-defects in the sample forming process, such as micropores, microcracks and so on, which will have a significant impact on the properties of the sample, but the effects of these defects are not considered in the simulation process. However, whether in experiment or finite element analysis, the elastic modulus of the structure decreases
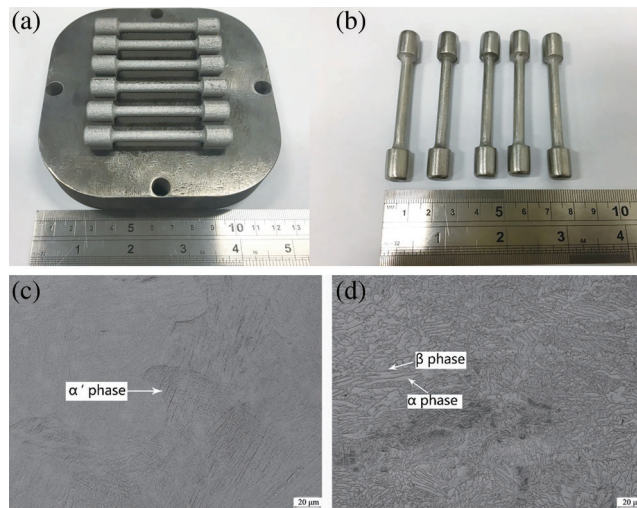
Figure 10: The tensile specimens manufactured by SLM: a) Tensile specimens (not polished), b) Tensile specimens (grinding, polishing), c) the microstructure of the Ti6Al4V sample with no heat treatment, d) the microstructure of the Ti6Al4V sample with heat treatment

Table 6: Mechanical properties of Ti6Al4V before and after heat treatment

	Tensile strength σ_b/MPa	Yield strength $\sigma_{0.2}$/MPa	Elongation rate δ/%
SLM	1238.7 ± 7.7	1043.9 ± 10.9	6.43 ± 0.29
SLM-Heat Treatment	1068.3 ± 26.7	1041.3 ± 17.7	10.18 ± 0.70
ASTM F136 (ISO 5832-3:2016)	≥860	≥795	≥10
Casting	≥895	≥825	≥6
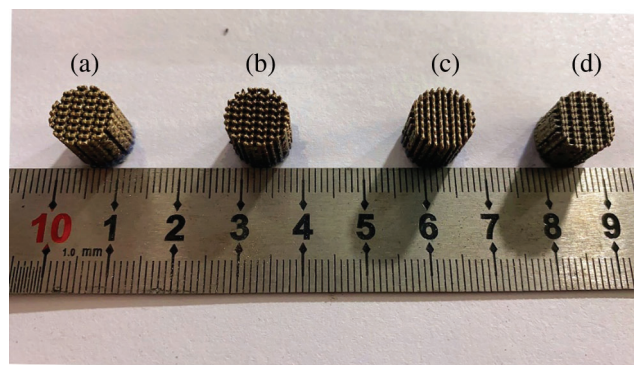
Figure 11: SLM manufacturing porous structure specimens, the porosity of specimens: (a) 69.34%, (b) 75.29%, (c) 80.41%, (d) 84.60%

with the increase of porosity, and has a good match with the elastic modulus of human bone. Due to the existence of defects, the strength of the experimental results and simulation results with the density of the trend is not consistent. Therefore, it is necessary to study the effect of micro defects on performance. On the other hand, some particles adhere to the surface of the strut, as shown in Figs. 8c and 13b, which

Table 7: Compressive yield strength and Elastic modulus of porous structure design specimens with different pores

Number	Porosity/%	Compressive strength σ_{bc}/MPa	Elastic modulus/Gpa
1	84.60	184.09	3.80
2	80.41	195.09	4.27
3	75.29	252.13	4.45
4	69.34	316.62	5.51

cause the surface and outline of the structure to be rough. At the same time, the uneven size of the molten pool will also lead to the uneven size of the pillar, which will eventually aggravate the stress concentration and reduce the mechanical properties. The above factors will affect and limit the mechanical properties of the porous structure, which leads to the difference between the simulation results and the measured results.

4.4 Ion Release Experiment

Before the ion release experiment, in order to simulate the real state of SLM manufactured implants, all the samples were treated by heat treatment, mirror polishing, and ultrasonic cleaning in ethanol and deionized water, and high-temperature sterilization.

The Ti6Al4V implants made by traditional casting process was selected as a control experiment. The experimental group was divided into control group (group N), casting titanium alloy implant group (NM group) and SLM titanium alloy implants group with 4 concentration gradients (SLM group). Each group carries on the experiment to not less than 3 batches of samples, the last test value takes the mean value.

SLM titanium alloy implant and cast titanium alloy implant were respectively immersed in serum-containing DMEM (Dulbecco's Modified Eagle Medium) according to the volume ratio of the surface area of the extracted specimen and the culture solution to 0.2 g/ml. In order to simulate the *in vivo* environment and get the accurate value of the ion release, DMEM was incubated at 37 and 5% carbon dioxide for 24 h, after filtration by a microporous membrane, the remaining culture medium in DMEM is the extraction solution containing metal ions.

Fig. 12 is the amount of ion release of Al and V extracted from SLM implant after surface polishing and the traditional process titanium alloy implant, in which the standard sample is 0.9% saline. As can be seen from Fig. 12a, it is difficult to detect the specific value of Al ion release in the SLM manufactured implant
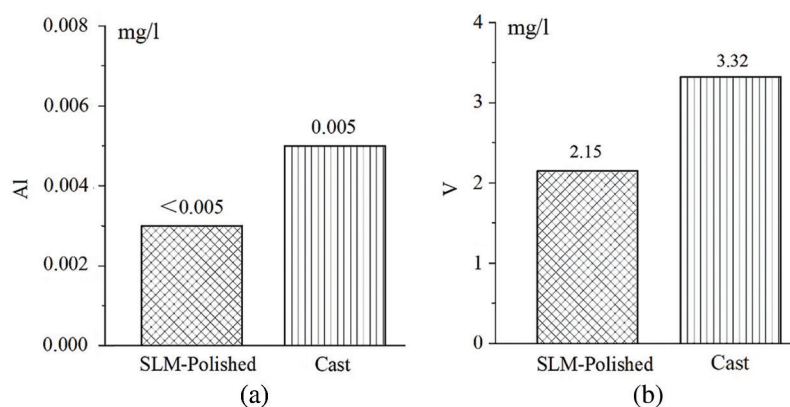
Figure 12: Ions release comparison between implant by SLM and Cast
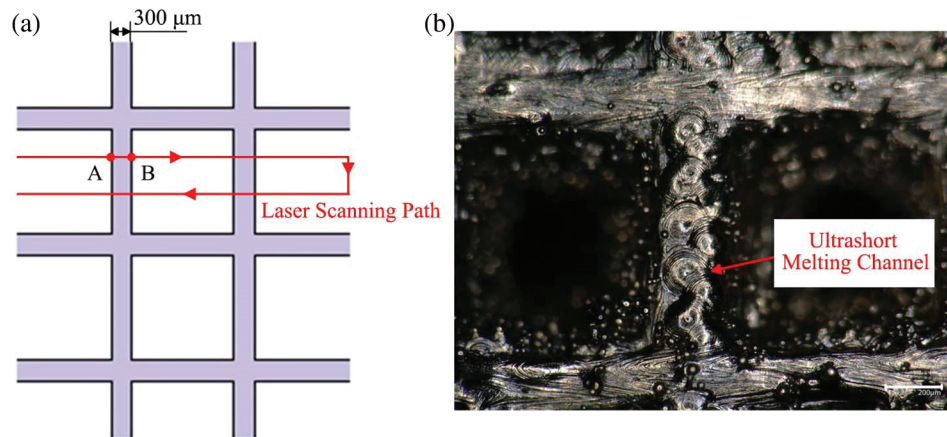
Figure 13: Laser scanning porous structure and powder adhesion: a) geometrical size of typical porous structure, b) enlarged microscopic image of porous structure

after surface polishing in 0.9% saline, but lower than that of the conventional process titanium alloy implant Al ion (0.005 mg/L); from Fig. 12b, the amount of V ion release (2.15 mg/L) of the SLM manufactured implant after heat treatment and surface treatment is also lower than that of the cast implant in normal saline (3.22 mg/L).Through this comparative experiment, it can be concluded that the SLM titanium alloy implant is more suitable for clinical application than the traditional titanium alloy implant in the toxic ion release.

4.5 Discussions

From the manufacturing effect, the Ti6Al4V vertebral implant is fine, the binding surface of the implant is well restrained and the manufacturing precision is high. However, there are still some problems that need to be improved in the manufacturing of spinal implants. An inevitable processing defect is the presence of powder adhesion at the edge of the porous structure during laser scanning. Fig. 13 shows laser scanning porous structure and followed by powder adhesion. As shown in Fig. 13a, the laser does not work until the scanning point reaches point A, and closes when it reaches point B, then the whole AB segment is scanned. The design distance of the AB segment is only 300 microns, and the laser scanning speed is 1000 mm/s. Therefore, the whole operation of opening and closing the laser in the entire AB segment needs to be completed within 0.3 ms. The short scanning line length and fast galvanometer scanning speed allow the powder near points A and B to receive sufficient laser energy, causing the powder to be incompletely molten, which causes powder adhesion. Fig. 13b shows the high-magnification electron microscopic morphology of the actual formed porous structure. It can be seen that the weld line is relatively clean when the length of the scanning line is long enough. Conversely, when the scan line length is short, the melt path is ellipsoidal and accompanied by significant powder adhesion, indicating that the laser scan time is extremely short. Therefore, for the SLM fabricating process of porous structure, it is important to optimize the scanner and laser delay to guarantee the surface quality.

The mechanical properties of this study are compared with the Ti6Al4V porous structure obtained by other additive manufacturing methodologies, as shown in Tab. 8. The elastic modulus obtained in this study is similar to that obtained by Wieding et al. [32] by selective laser melting, but the compressive strength is higher. Overall, the compressive strength and elastic modulus of this study are higher than other research results, the main reason is that different structural features lead to differences in mechanical properties.

Table 8: Comparison of mechanical properties of additively manufactured Ti-6Al-4V scaffolds

Manufacturing technology	Structural features	Porosity (%)	Compressive strength (MPa)	Elastic modulus (GPa)	References
Powder metallurgic	–	80	40	2.87	[30]
Electron beam melting, EBM	Homogeneously porous	65	110	2.7	[31]
	Gradient porous	45.6	366.5	64.8	
Selective laser melting, SLM	Scaffold with rectangular struts	71.9	145	3.7	[32]
	Scaffold with shifted struts	70.2	155	5.1	
Selective laser sintering, SLS	Low porosity	70	–	2.6	[33]
	Medium porosity	38.5	–	3.5	
	High porosity	16.2	–	3.7	
Three dimensional printing, 3DP	Homogeneously porous	33	47	2.0	[34]
	Homogeneously porous	33	90	3.3	

There are still some designing problems need to be addressed in the next stage:

1. The transverse width of the vertebral implant is too large. The transverse width of the fixed plate is even larger than the transverse width of the atlas junction surface, and the incision is large when used in clinical operation, which will have a greater impact on patient. Therefore, in the process of implant design, the atlas joint surface can be as narrow as possible under the condition of using requirements, and the transverse width of the fixed plate is also as small as possible.

2. The thickness of the fixed plate of the implant was 1.8 mm, and the guiding effect was not enough when the screw was fixed. The structures around the spine are complex and the vessels and nerves are abundant. Therefore, the screws must be inserted into the pedicle to avoid the nerves and blood vessels when the screws are fixed. When the thickness of the fixed plate is insufficient to guide the screw fix, the difficulty of fixing screw accurately is increased. Therefore, in the design process, screw fixing orientation should be taken into full consideration or increasing the thickness of the fixed plate so as to increase the guidance, or take a set of navigation templates that match the implant to ensure accurate fixing of screws.

In addition, the model data processing and manufacturing process also have the following needs to be improved:

1. For the complex porous structure, an effective and easy-removed support structure should be constructed in the SLM manufacturing process. In this paper, considering the complexity of the porous structure, the conventional support is not set, but the porous structure is directly extended to support the role. Although the structural effect of this support is obvious, it is difficult to remove the support, and more traditional techniques are needed to support it. Therefore, it is necessary to design an effective and easy to remove support for porous structure.

2. The actual hole size of porous structure has deviation. The first stage hole diameter is 0.75 mm, and the second stage hole diameter is 1.5 mm. The first stage hole size and the second stage hole size are reduced in different degrees after actual manufacturing. This is due to the phenomenon of powder bonding affected the width of the channel, resulting in the actual hole size smaller than the design size, as shown in Fig. 7. Therefore, the design aperture should be adjusted properly to ensure the actual aperture can meet the requirements when the aperture has strict size requirements.

3. Finally, since the spinal implants are ultimately used for clinical purposes, the design process should also give full consideration to the doctor's recommendations on actual operations. At the same time, the design process should also comply with the principles and methods of SLM manufacturing, for example: the minimum design structure size should be greater than the minimum spot size.

5 Conclusions

1. The Ti6Al4V bionic porous spinal implant was manufactured by computer-aided design and SLM technology. The manufacturing effect was good, and the result of matching with the spinal model of photosensitive resin 3D printing was ideal. However, the pore structure has not been optimized, through the finite element analysis, we can see that there is stress concentration in the structure, so the follow-up research work should also optimize the pore structure in order to reduce the stress concentration.

2. In order to ensure the quality of implant, the binding surface should be avoided to be overhang as far as possible. after SLM manufacturing, the implant surface roughness is 15 μm, the micro-hardness of molding surface is HV 373, the tensile strength σ_b = 1238.7 MPa, yield strength $\sigma_{0.2}$ = 1043.9 MPa, the elongation rate is 6.43%, the compressive strength of porous structure with 84.60% porosity is 142.99 MPa. In the concentration of 0.9% saline, after heat treatment and polishing treatment, the amount of Al ion release of SLM implant is less than 0.005 mg/l, and the amount of V ion release is 2.15 mg/l, which is more suitable for clinical application than titanium alloy implant made by traditional casting process. At the same time, the elastic modulus of the porous structure formed by SLM is lower than 6 Gpa, which makes the porous structure have better adaptability to human bones.

3. The design and SLM manufacturing of spinal implant need further optimization. For example, the width of the implant should be reduced as far as possible to reduce the damage to the patient; the fixed plate should be set reasonable structure to ensure the accuracy of navigation.

Conflicts of Interest: The authors declare that they have no conflicts of interest to report regarding the present study.

References

1. Wang, S. J., Han, Y. C., Liu, X. M., Ma, B., Zhao, W. D. et al. (2014). Fusion techniques for adult isthmic spondylolisthesis: a systematic review. *Archives of Orthopaedic and Trauma Surgery, 134(6),* 777–784. DOI 10.1007/s00402-014-1985-9.

2. Cloward, R. B. (1988). The anterior surgical approach to the cervical spine: the cloward procedure: past, present, and future. *Presidential Guest Lecture, Cervical Spine Research Society Spine, 13(7),* 823–827.

3. Gu, D., He, B. (2016). Finite element simulation and experimental investigation of residual stresses in selective laser melted Ti-Ni shape memory alloy. *Computational Materials Science, 117(6),* 221–232. DOI 10.1016/j. commatsci.2016.01.044.

4. Vrancken, B., Thijs, L., Kruth, J. P., Van Humbeeck, J. (2012). Heat treatment of Ti6Al4V produced by selective laser melting: microstructure and mechanical properties.. *Journal of Alloys and Compounds, 541,* 177–185. DOI 10.1016/j.jallcom.2012.07.022.

5. Wei, Q., Li, S., Han, C., Li, W., Cheng, L. et al. (2015). Selective laser melting of stainless-steel/nano-hydroxyapatite composites for medical applications: microstructure, element distribution, crack and mechanical properties. *Journal of Materials Processing Technology, 222,* 444–453. DOI 10.1016/j.jmatprotec.2015.02.010.

6. Li, R., Liu, J., Shi, Y., Wang, L., Jiang, W. (2012). Balling behavior of stainless steel and nickel powder during selective laser melting process. *International Journal of Advanced Manufacturing Technology, 59(9–12),* 1025–1035. DOI 10.1007/s00170-011-3566-1.

7. Wang, D., Wang, Y., Wu, S., Lin, H., Yang, Y. et al. (2017). Customized a Ti6Al4V bone plate for complex pelvic fracture by selective laser melting. *Materials, 10(1),* 35. DOI 10.3390/ma10010035.

8. Tewari, M. K., Gifti, D. S., Singh, P., Khosla, V. K., Mathuriya, S. N. et al. (2005). Diagnosis and prognostication of adult spinal cord injury without radiographic abnormality using magnetic resonance imaging: analysis of 40 patients. *Surgical Neurology, 63(3),* 204–209. DOI 10.1016/j.surneu.2004.05.042.

9. Lin, P. M., Cautilli, R. A., Joyce, M. F. (1983). Posterior lumbar interbody fusion. *Clinical Orthopaedics and Related Research, 180,* 154–168.

10. Dvorak, M. F., Kwon, B. K., Fisher, C. G., Eiserloh, H. L., Boyd, M. et al. (2003). Effectiveness of titanium mesh cylindrical cages in anterior column reconstruction after thoracic and lumbar vertebral body resection. *Spine, 28 (9),* 902–908.

11. Heo, W., Kang, D. H., Park, K. B., Hwang, S. H., Park, I. S. et al. (2011): Is titanium mesh cage safe in surgical management of pyogenic spondylitis. *Journal of Korean Neurosurgical Society, 50(4),* 357–362. DOI 10.3340/jkns.2011.50.4.357.

12. Weiner, B. K., Fraser, R. D. (1998). Spine update lumbar interbody cages. *Spine, 23(5),* 634–640. DOI 10.1097/00007632-199803010-00020.

13. Cho, D. Y., Lee, W. Y., Sheu, P. C. (2004). Treatment of multilevel cervical fusion with cages. *Surgical Neurology, 62(5),* 378–385. DOI 10.1016/j.surneu.2004.01.021.

14. Kokubo, T., Kim, H. M., Kawashita, M. (2003). Novel bioactive materials with different mechanical properties. *Biomaterials, 24(13),* 2161–2175. DOI 10.1016/S0142-9612(03)00044-9.

15. Suzuki, T., Abe, E., Miyakoshi, N., Murai, H., Shimada, Y. (2012). Anterior decompression and shortening reconstruction with a titanium mesh cage through a posterior approach alone for the treatment of lumbar burst fractures. *Asian Spine Journal, 6(2),* 123–130. DOI 10.4184/asj.2012.6.2.123.

16. Martijn van Dijk, M. D., Smit, T. H., Burger, E. H., Wuisman, P. I. (2002). Bioabsorbable poly-l-lactic acid cages for lumbar interbody fusion: three-year follow-up radiographic, histologic, and histomorphometric analysis in goats. *Spine, 27(23),* 2706–2714. DOI 10.1097/00007632-200212010-00010.

17. Levine, B. R., Sporer, S., Poggie, R. A., Valle, C. J. D., Jacobs, J. J. (2006). Experimental and clinical performance of porous tantalum in orthopedic surgery. *Biomaterials, 27(27),* 4671–4681. DOI 10.1016/j. biomaterials.2006.04.041.

18. Jung, H. D., Yook, S. W., Jang, T. S., Li, Y., Kim, H. E. et al. (2013). Dynamic freeze casting for the production of porous titanium (Ti) scaffolds. *Materials Science and Engineering: C, 33(1),* 59–63. DOI 10.1016/j. msec.2012.08.004.

19. Jiang, G., He, G. (2014). Enhancement of the porous titanium with entangled wire structure for load-bearing biomedical applications. *Materials & Design, 56,* 241–244. DOI 10.1016/j.matdes.2013.11.019.

20. Over, C., Meiners, W., Wissenbach, K., Lindemann, M., Hammann, G. (2001). Selective laser melting: a new approach for the direct manufacturing of metal parts and tools. *Proceedings of the International Conferences on LANE, Fürth, Germany,* pp. 391–398.

21. Kasperovich, G., Haubrich, J., Gussone, J., Requena, G. (2016). Correlation between porosity and processing parameters in TiAl6V4 produced by selective laser melting. *Materials & Design, 105,* 160–170. DOI 10.1016/j.matdes.2016.05.070.

22. Zhang, L. C., Attar, H. (2016). Selective laser melting of titanium alloys and titanium matrix composites for biomedical applications: a review. *Advanced Engineering Materials, 18(4),* 463–475. DOI 10.1002/adem.201500419.

23. Karageorgiou, V., Kaplan, D. (2005). Porosity of 3D biomaterial scafolds and osteogenesis. *Biomaterials, 26(27),* 5474–5491. DOI 10.1016/j.biomaterials.2005.02.002.

24. Maas, S. A., Ellis, B. J., Rawlins, D. S., Weiss, J. A. (2016). Finite element simulation of articular contact mechanics with quadratic tetrahedral elements. *Journal of Biomechanics, 49(5),* 659–667. DOI 10.1016/j.jbiomech.2016.01.024.

25. Ye, Z. H. (2014). *The personalized design and process research of selective laser melting manufacturing of Ti6Al4V tibial implant (M.D. Thesis)*. South China University of Technology, China.

26. Eisenbarth, E., Linez, P., Biehl, V., Velten, D., Breme, J. et al. (2002). Cell orientation and cytoskeleton organisation on ground titanium surfaces. *Biomolecular Engineering, 19(2–6),* 233–237. DOI 10.1016/S1389-0344(02)00028-X.

27. Yadroitsev, I., Thivillon, L., Bertrand, P., Smurov, I. (2007). Strategy of manufacturing components with designed internal structure by selective laser melting of metallic powder. *Applied Surface Science, 254(4),* 980–983. DOI 10.1016/j.apsusc.2007.08.046.

28. Matsumoto, M., Shiomi, M., Osakada, K., Abe, F. (2002). Finite element analysis of single layer forming on metallic powder bed in rapid prototyping by selective laser processing. *International Journal of Machine Tools and Manufacture, 42(1),* 61–67. DOI 10.1016/S0890-6955(01)00093-1.

29. Vandenbroucke, B., Kruth, J. P. (2013). Selective laser melting of biocompatible metals for rapid manufacturing of medical parts. *Rapid Prototyping Journal, 13(4),* 196–203. DOI 10.1108/13552540710776142.

30. Wen, C. E., Yamada, Y., Shimojima, K., Chino, Y., Asahina, T. et al. (2002). Processing and mechanical properties of autogenous titanium implant material. *Journal of Materials Science Materials in Medicine, 13(4),* 397–401. DOI 10.1023/A:1014344819558.

31. Varma, A., Li, B., Mukasyan, A. (2002). Novel synthesis of orthopaedic implant materials. *Advanced Engineering Materials, 4(7),* 482–487. DOI 10.1002/1527-2648(20020717)4:7<482::AID-ADEM482>3.0.CO;2-8.

32. Wieding, J., Jonitz, A., Bader, R. (2012). The effect of structural design on mechanical properties and cellular response of additive manufactured titanium scaffolds. *Materials, 5(8),* 1336–1347. DOI 10.3390/ma5081336.

33. Cheng, A., Humayun, A., Cohen, D. J., Boyan, B. D., Schwartz, Z. (2014). Additively manufactured 3d porous Ti-6Al-4V constructs mimic trabecular bone structure and regulate osteoblast proliferation, differentiation and local factor production in a porosity and surface roughness dependent manner. *Biofabrication, 6(4),* 045007. DOI 10.1088/1758-5082/6/4/045007.

34. Barui, S., Chatterjee, S., Mandal, S., Kumar, A., Basu, B. (2017). Microstructure and compression properties of 3d powder printed ti-6al-4v scaffolds with designed porosity: experimental and computational analysis. *Materials Science & Engineering: C, 70,* 812–823. DOI 10.1016/j.msec.2016.09.040.